ADCS Design for a Sounding Rocket with Thrust Vectoring

Pedro dos Santos
pedrodossantos31@tecnico.ulisboa.pt

Instituto Superior Técnico, Universidade de Lisboa, Portugal

December 2022

Abstract

This paper addresses the development of an attitude determination and control system (ADCS) for a sounding rocket using Thrust Vector Control (TVC). To design the ADCS, a non-linear six-degrees-of-freedom model for the rocket dynamics and kinematics is deduced and implemented in simulation environment. An optimal attitude controller is designed using the linear quadratic regulator (LQR) with an additional integral action, and relying on the derived linear, time-varying, state-space representation of the rocket. The controller is tested in the simulation environment, demonstrating satisfactory attitude tracking performance, and robustness to model uncertainties. A linear parameter estimator is implemented to provide real-time estimates on the aerodynamic forces and moments. These estimates are used by an adaptive controller that computes the gains in real-time after correcting the state-space model. Finally, a navigation system is designed, based on measurements available onboard, to provide accurate estimates on the rocket's state. The ADCS is the result of the integration of the attitude control and navigation systems, with the complete system being implemented and tested in simulation, and demonstrating satisfactory performance.

Keywords: ADCS, Sounding rocket, TVC, Attitude control, Attitude estimation

1. Introduction

The main motivation behind this work is the development of an attitude determination and control system (ADCS) for a future sounding rocket from a student rocketry team from Instituto Superior Técnico (IST), named Rocket Experiment Division (RED). The designed attitude control system assumes that the rocket uses Thrust Vector Control (TVC) technology as the actuation method, and aims to control the rocket's pitch and yaw angles. The roll angle is assumed to be controlled by an additional roll control system whose design is out of the scope of this work.

During the atmospheric flight phase of a rocket, stabilization can be achieved through the use of aerodynamic fins. With a correct design of the fins, the vehicle can be naturally stable [1]. However, the rocket is subjected to various external disturbances, such as wind gusts, which prevent the vehicle to follow a desirable, pre-calculated trajectory or, even more intense, completely destabilize it [2]. It is then clear the necessity of having an active attitude control and stabilization system that not only ensures the stability of the rocket, but allows to actively correct its trajectory in order to achieve specific mission goals. As for the actuation method, Thrust Vector Control (TVC), or thrust vectoring for short, is used by most launch vehicles and works by redirecting the thrust vector in order to create a control torque [3]. With respect to other actuation techniques, like actively controlled fins, TVC allows for a wider range of operating conditions and provides better efficiency [4]. The control system design tends to be very conservative in the aerospace industry. Restricting the dynamic analysis to accommodate more sophisticated control design techniques risks the later realization that such restrictions would have to be lifted and would invalidate the control design. Among the classical techniques, the Proportional-Integral-Derivative (PID) control is on the core of most commonly used launch vehicle control systems [3, 5]. Although widely used, PID control has its downsides when it comes to robustness and external disturbances rejection [6]. The problem of controlling ascending launch vehicles is dominated by parameter uncertainty, which in face of the lack of robustness of the PID controller may be a concerning issue. Moreover, the rocket flight parameters considerably change throughout the flight. To overcome this, gain scheduling techniques have been proposed, that rely on the linearization of the dynamics at different operating conditions. Still in the linear domain, the use of optimal controllers, such as the LQR, provides more robustness and ensures an optimal solution for a given cost function [6, 7]. As a way to improve the

robustness of linear time-varying controllers, real-time parameter estimators can be introduced in the control loop to form an adaptive control system. The online identification of system parameters allows the controller to act on a more accurate representation of the system dynamics [8].

This work has several contributions, always having in mind the reliability and robustness of the proposed solutions: a six degrees-of-freedom (6 DoF) non-linear model for the dynamics and kinematics of a rocket, that serves as a tool for control and navigation system design; a generic state-space representation for linear and optimal control design; an optimal pitch and yaw controller resorting to the LQR technique; a linear time-varying parameter estimator to estimate in real time the aerodynamic forces and moments acting on the vehicle; and a navigation system, based on measurements available on-board, to provide accurate estimates on the rocket's state.

2. Rocket Dynamics and Kinematics Modelling

To design the ADCS, a mathematical model that represents the translational and rotational dynamics and kinematics of the rocket is necessary.

2.1. Assumptions

Some assumptions are used to derive the model: **the rocket is considered to be a rigid body**, meaning no elastic behaviours are modelled; **the rocket is assumed to be axially symmetric, as well as the mass allocation**, which means that the principal inertia axes coincide with the body axes, the centre of mass is on the longitudinal axis, and the aerodynamic behaviour is identical in both the pitch and yaw planes; and **the flat Earth model is used**, meaning that neither the curvature nor rotation of the Earth are taken into account.

2.2. Reference frames

To describe the dynamics and kinematics of the rocket, it is crucial to define the reference frames to be used. Two reference frames are used: a body-fixed one, where the equations of motion are written; and an inertial space-fixed one. The body-fixed reference frame has its origin located in the center of mass of the vehicle, as shown in Fig. 1.

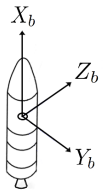

Figure 1: Body-fixed reference frame.

The x-axis (X_b) is along the rocket's longitudinal axis, while the z-axis (Z_b) and y-axis (Y_b) complete the orthogonal reference frame. As for the inertial space-fixed reference frame, given that neither the curvature nor the rotational motion of the Earth are taken into account, a simple orthogonal frame centered in the launch location is used. The x-axis (X_e) is pointing upwards, so that for a zero inclination launch the x-axes of both reference frames are aligned; and the other two axes (Y_e and Z_e) are preferably aligned with a pair of cardinal directions.

With the reference frames detailed, it is necessary to define the coordinate transformation between both reference frames. This is done by using a sequential rotation of the body frame relative to the Earth frame defined by the three Euler angles:

$$R(\phi, \theta, \psi) = R_z(\psi) \cdot R_y(\theta) \cdot R_x(\phi)\,, \qquad (1)$$

where ϕ is the Euler angle of rotation of the body around the x-axis of the Earth frame, also known as roll; θ is the Euler angle of rotation of the body around the y-axis of the Earth frame, also known as pitch; and ψ is the Euler angle of rotation of the body around the z-axis of the Earth frame, also known as yaw.

The Euler angles describe the attitude of the rocket, representing the variables to be controlled by the attitude control system. The coordinate transformation from the body frame to the Earth frame is then defined by the following transformation matrix:

$$\mathbf{R} = \begin{bmatrix} c_\theta c_\psi & s_\phi s_\theta c_\psi - c_\phi s_\psi & c_\phi s_\theta c_\psi + s_\phi s_\psi \\ c_\theta s_\psi & s_\phi s_\theta s_\psi + c_\phi c_\psi & c_\phi s_\theta s_\psi - s_\phi c_\psi \\ -s_\theta & s_\phi c_\theta & c_\phi c_\theta \end{bmatrix} \qquad (2)$$

where c and s stand as abbreviations for the trignometric functions. The inverse transform, from the Earth frame to the body frame, is defined by the transpose ($\mathbf{R}^T$).

2.3. External Forces and Moments

From the dynamic point of view, sounding rockets experience four main forces during a flight: Weight, Thrust, and the aerodynamic forces - Lift and Drag.

2.3.1. Gravity model

Using the flat Earth model assumption, the gravitational acceleration is considered to vary only with altitude. This variation is given by:

$$g = g_0 \frac{R_E^2}{(R_E + h)^2}\,, \qquad (3)$$

where g_0 is the gravitational acceleration constant at surface level, R_E is the mean Earth radius and h is the altitude. The gravitational force in the Earth-fixed reference frame is equal to

$${}^{E}\mathbf{F_g} = \begin{bmatrix} -mg \\ 0 \\ 0 \end{bmatrix}\,, \qquad (4)$$

and the transformation matrix is used to translate it into the body frame:

$$ {}^{B}\mathbf{F_g} = \begin{bmatrix} -mg \cdot c_\theta c_\psi \\ -mg \cdot (s_\phi s_\theta c_\psi - c_\phi s_\psi) \\ -mg \cdot (c_\phi s_\theta c_\psi + s_\phi s_\psi) \end{bmatrix} . \tag{5} $$

2.3.2. Propulsion model

The propulsion model was derived using equations mainly obtained from [4], considering ideal propulsion and all its underlying assumptions. The thrust produced by the rocket motor is simply

$$ T = \underbrace{|\dot{m}| \cdot v_e}_{\text{Dynamic}} + \underbrace{(p_e - p_a) \cdot A_e}_{\text{Static}} , \tag{6} $$

where $\dot{m}$ is the mass flow rate, v_e is the effective exhaust velocity, p_e is the nozzle exit pressure, p_a is the atmospheric pressure, and A_e is the nozzle exit area. two separate contributions can be identified: the dynamic one, caused by the exhaust of the expanded combustion gases; and the static, caused by the pressure gradient between the nozzle exit and the atmosphere.

Considering that the most common propulsion technology for sounding rockets is solid propulsion, and that it is the technology used by RED, a model that uses the internal combustion equations and the solid propellant characteristics is implemented to calculate the thrust produced by the motor (T) and the associated mass flow rate ($\dot{m}$).

2.3.3. TVC actuation

By controlling the direction of the thrust force (or vector), TVC actuation produces torques that act on the rocket's centre of mass, influencing its rotation in pitch and yaw. The decomposition of the propulsive force in the three body axes can be done as illustrated in Fig. 2. According to it, the thrust

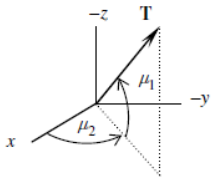

Figure 2: Thrust vector decomposition in the body axes [7].

vector is decomposed using the angles μ_1 and μ_2, where μ_1 is the gimbal angle that, on its own, produces a pitching moment, and μ_2 is the one that produces a yawing moment. Using these angles, the propulsive force in the body frame follows [7],

$$ {}^{B}\mathbf{F_p} = \begin{bmatrix} T \cos\mu_1 \cos\mu_2 \\ -T \cos\mu_1 \sin\mu_2 \\ -T \sin\mu_1 \end{bmatrix} , \tag{7} $$

while the control moment in the body frame, produced by thrust vectoring, is

$$ {}^{B}\mathbf{M_p} = \begin{bmatrix} 0 \\ -T \sin\mu_1 \, l \\ T \cos\mu_1 \sin\mu_2 \, l \end{bmatrix} , \tag{8} $$

where l is the moment arm, which corresponds to the distance between the nozzle gimbal point and the centre of mass of the rocket.

2.3.4. Aerodynamic Forces and Moments

The rocket will be subjected to aerodynamic forces and moments resulting from its interaction with the fluid medium composing the atmosphere. Starting by the forces, they are expressed in the body axes according to

$$ {}^{B}\mathbf{F_a} = \begin{bmatrix} -\overline{q}\, C_A \, S \\ \overline{q}\, C_Y \, S \\ -\overline{q}\, C_N \, S \end{bmatrix} , \tag{9} $$

where C_A is the axial aerodynamic force coefficient, C_Y is the lateral aerodynamic force coefficient, C_N is the normal aerodynamic force coefficient, $\overline{q}$ is the dynamic pressure and S is a reference area, usually corresponding to the cross sectional area of the fuselage. The axial and normal aerodynamic forces correspond to the body axes components of Lift and Drag, and are related through the aerodynamic angles - the angle of attack and the sideslip angle,

$$ \alpha = \arctan\left(\frac{w_{rel}}{u_{rel}}\right), \beta = \arcsin\left(\frac{v_{rel}}{V_{rel}}\right), \tag{10} $$

where u_{rel}, v_{rel}, and w_{rel} are the components of the relative velocity vector with respect to the wind velocity.

The force coefficients can be determined using a linear relation with the aerodynamic angles, whose derivative depends mainly on the angle itself and Mach number,

$$ C_Y = C_{Y\beta}\,\beta, \quad C_N = C_{N\alpha}\,\alpha\,. \tag{11} $$

As for the aerodynamic moments, in the body axes they are given by

$$ {}^{B}\mathbf{M_a} = \begin{bmatrix} \overline{q}\, C_l \, S \, d \\ \overline{q}\, C_m \, S \, d \\ \overline{q}\, C_n \, S \, d \end{bmatrix} , \tag{12} $$

where d is a reference length, usually corresponding to the diameter of the fuselage. If the reference moment station is defined as the centre of pressure, and its location can be determined, the reference moments are zero and the moment coefficients take

the following form

$$C_l = \frac{d}{2V_{rel}} C_{lp}\, p\,, \tag{13a}$$

$$C_m = -C_N\, SM + \frac{d}{2V_{rel}} \left(C_{m_q} + C_{m_{\dot{\alpha}}}\right) q\,, \tag{13b}$$

$$C_n = -C_Y\, SM + \frac{d}{2V_{rel}} \left(C_{n_r} + C_{n_{\dot{\beta}}}\right) r\,, \tag{13c}$$

where the static stability margin ($SM = \frac{x_{cp} - x_{cm}}{d}$) intuitively appears, p, q, and r, are the angular velocities, and C_{l_p}, C_{m_q}, $C_{m_{\dot{\alpha}}}$, C_{n_r}, and $C_{n_{\dot{\beta}}}$ are all aerodynamic damping coefficients.

2.4. 6 DoF equations of motion

2.4.1. Translational motion

By applying Newton's second law, and taking into account that the body frame is a rotating, we obtain

$${}^{B}\dot{\mathbf{v}} = \frac{1}{m}\left({}^{B}\mathbf{F_g} + {}^{B}\mathbf{F_p} + {}^{B}\mathbf{F_a}\right) - \mathbf{S}(\boldsymbol{\omega})\ {}^{B}\mathbf{v}\,, \tag{14}$$

where $\mathbf{S}(.)$ is a skew-symmetric matrix, and the mass derivative term has been included in the propulsive force. By substituting the external forces in (14), the dynamics can be particularized in the body acceleration components:

$$\begin{cases} \dot{u} = -g\, c_\theta\, c_\psi - \dfrac{\overline{q}}{m} S\, C_A \\ \quad + \dfrac{T}{m} c_{\mu_1}\, c_{\mu_2} - q\, w + r\, v \\ \dot{v} = -g\left(s_\phi\, s_\theta\, c_\psi - c_\phi\, s_\psi\right) + \dfrac{\overline{q}}{m} S\, C_Y \\ \quad - \dfrac{T}{m} c_{\mu_1}\, s_{\mu_2} - r\, u + p\, w \\ \dot{w} = -g\left(c_\phi\, s_\theta\, c_\psi + s_\phi\, s_\psi\right) - \dfrac{\overline{q}}{m} S\, C_N \\ \quad - \dfrac{T}{m} s_{\mu_1} - p\, v + q\, u \end{cases} \tag{15}$$

2.4.2. Rotational motion

Euler's equation for rigid body rotational motion yields

$${}^{B}\mathbf{M} = \mathbf{J}\,\dot{\boldsymbol{\omega}} + \boldsymbol{\omega} \times \mathbf{J}\,\boldsymbol{\omega}\,, \tag{16}$$

where $\mathbf{J}$ is the inertia matrix. Following the axial symmetry assumption, the cross-products of inertia can be assumed as zero and the y and z terms can be assumed equal, resulting in

$$\mathbf{J} = diag(J_l, J_t, J_t)\,, \tag{17}$$

where J_l denotes the longitudinal inertia and J_t denotes the transverse inertia. By substituting the inertia matrix $\mathbf{J}$ and the external moment in the body frame ${}^{B}\mathbf{M}$ in (16), the explicit dynamics are obtained in terms of the body angular acceleration components:

$$\begin{cases} \dot{p} = {J_l}^{-1}\left(\overline{q}\, S\, d\, C_l + \tau_r + \mu_r\right) \\ \dot{q} = {J_t}^{-1}\left(\overline{q}\, S\, d\, C_m - T\, s_{\mu_1}\, l\right) \\ \dot{r} = {J_t}^{-1}\left(\overline{q}\, S\, d\, C_n + T\, c_{\mu_1}\, s_{\mu_2}\, l\right) \end{cases} \tag{18}$$

where μ_r represents the rolling moment caused by the additional roll control system and τ_r accounts for external disturbances. Finally, the rotational kinematics are given by the time derivative of the Euler angles [9]:

$$\begin{cases} \dot{\phi} = p + \left(q\, s_\phi + r\, c_\phi\right) t_\theta \\ \dot{\theta} = q\, c_\phi - r\, s_\phi \\ \dot{\psi} = \dfrac{q\, s_\phi + r\, c_\phi}{c_\theta} \end{cases} \tag{19}$$

It is noted that by using the Euler angles a singularity arises for $\theta = \pm\frac{\pi}{2}$, however, the way the reference frames are defined prevents the rocket to reach this attitude inside the admissible range of operation. By grouping (15), (18), and (19) the 6 DoF non-linear model of the rocket is fully defined.

3. Preliminary Rocket Design

In order to test and validate the proposed ADCS it is necessary to use a reference rocket model. In this way, a preliminary design for a future RED's rocket with Thrust Vector Control is performed. The rocket is designed to have a burning phase coinciding with the full duration of the climb, so that TVC can be used to control its attitude up to apogee. Additionally, it is required that the terminal velocity is inside a safe range to allow the correct activation of the recovery system. To meet these design goals, the solid motor characteristics are iteratively tested using the developed propulsion model, and the flight for a vertical trajectory is simulated resorting to the simulation model. Tables 1 and 2 respectively present the main rocket characteristics and the simulation results.

Table 1: Main rocket characteristics.

Total mass	82.9 kg
Dry mass	40.0 kg
Length	3.57 m
Max diameter	24 cm

Table 2: Simulation results for a vertical trajectory.

Apogee	4945 m
Max velocity	82 m/s
Max acceleration	1.7 m/s^2
Time to apogee	100 s
Velocity at burnout	27 m/s
Vertical distance after burnout	38 m

4. Attitude Control System Design

4.1. Model Linearization

To design an optimal, linear controller, it is necessary to obtain a linear version of the model and respective state-space representation. The non-linear model can be linearized at equilibrium points of

the system by using a Taylor series expansion, considering small perturbations. For the case of a rocket, conditions change considerably throughout the flight, hence, it is not correct to choose a single equilibrium point to linearize the system. Instead, a nominal trajectory is selected and the system is linearized at multiple operating points. The outcome is a linear time-variant system.

When obtaining the linear version of the system, it is advantageous to consider some assumptions: the roll rate (p) is considered to be zero as it will be controlled by an external roll control system, reducing the order of the system by one; the wind is assumed to be zero, allowing to directly use the linear velocity in the body frame in the aerodynamic terms; the actuator dynamics are not included in the model; and the system parameters are considered to be constant at the linearization points, removing the dependencies on the state variables when computing the Taylor derivatives. By applying this Taylor series expansion to the non-linear system around the operating points, a linear time-variant system in the perturbation domain is obtained, that can be represented in the state-space form:

$$\delta\mathbf{x} = [\delta u, \delta v, \delta w, \delta q, \delta r, \delta\phi, \delta\theta, \delta\psi]^T\,, \tag{20a}$$

$$\delta\mathbf{u} = [\delta\mu_1, \delta\mu_2]^T\,, \tag{20b}$$

$$\delta\dot{\mathbf{x}}(t) = \mathbf{A}(t)\cdot\delta\mathbf{x}(t) + \mathbf{B}(t)\cdot\delta\mathbf{u}(t)\,, \tag{20c}$$

where $\mathbf{A}(t)$ and $\mathbf{B}(t)$ are the state-space matrices given by the first-order Taylor derivatives with respect to system states and inputs, respectively, calculated at the operating points.

4.1.1. Nominal Trajectory

Regarding the attitude reference that defines the nominal trajectory, a varying pitch trajectory, in which the controller restricts the motion to the pitch plane (yaw equal to zero) and makes the rocket deviate from the vertical to later recover it, is selected. In this way, it is ensured that the apogee is reached further away from the launch site, increasing safety. Figure 3 shows the nominal pitch angle and rate over time.

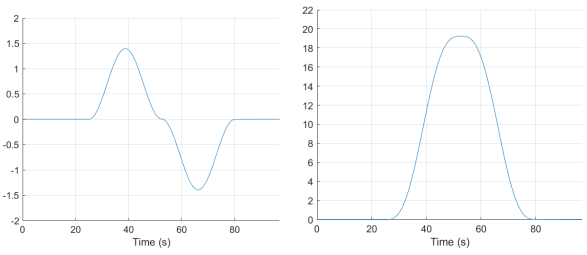

(a) Pitch rate (°/s) (b) Pitch angle (°)

Figure 3: Nominal Pitch rate and angle over time.

Since the system is naturally unstable, it is necessary to find the time evolution of the nominal control inputs that allows the rocket to nominally follow the trajectory, defined by an attitude reference over time. This is done by using a PID controller that in simulation, without perturbations, is able to stabilize the vehicle and track the attitude reference. The input values over time are then stored to use as predetermined feedforward control inputs.

4.1.2. Linearization Results

It is possible to identify two distinct sections of the nominal trajectory: a first section up to $t = 25\,\mathrm{s}$ in which motion is strictly vertical, and a second section up to burnout in which pitch is varying. In the vertical section, we have that: $\phi_0 = \theta_0 = \psi_0 = 0$, $v_0 = w_0 = 0$, $q_0 = r_0 = 0$, and $\mu_{1_0} = \mu_{2_{0=0}}$. This results in a simplified version of the state-space representation, for which the longitudinal and lateral modes are decoupled, and δu and $\delta\phi$ are no longer states:

$$\delta\mathbf{x}_{lon} = [\delta w, \delta q, \delta\theta]^T, \qquad \delta\mathbf{u}_{lon} = [\delta\mu_1]\,; \tag{21a}$$

$$\delta\mathbf{x}_{lat} = [\delta v, \delta r, \delta\psi]^T, \qquad \delta\mathbf{u}_{lat} = [\delta\mu_2]\,. \tag{21b}$$

For the varying pitch section, we have that: $\phi_0 = \psi_0 = 0$, $v_0 = 0$, $r_0 = 0$, and $\mu_{2_{0=0}}$. This results in a simplified version of the state-space representation, for which the longitudinal and lateral modes are also decoupled:

$$\delta\mathbf{x}_{lon} = [\delta u, \delta w, \delta q, \delta\theta]^T, \qquad \delta\mathbf{u}_{lon} = [\delta\mu_1] \tag{22a}$$

$$\delta\mathbf{x}_{lat} = [\delta v, \delta r, \delta\phi, \delta\psi]^T, \qquad \delta\mathbf{u}_{lat} = [\delta\mu_2] \tag{22b}$$

4.1.3. Modal Analysis

It is important to determine the location of the system poles throughout the nominal trajectory to derive the open-loop stability. For a time-varying system, the stability is not mathematically guaranteed with this method, however, the study is carried out to understand the behaviour of the systems throughout the flight. Figure 4 details the pole evolution (from blue to green) up to $t = 25\,\mathrm{s}$.

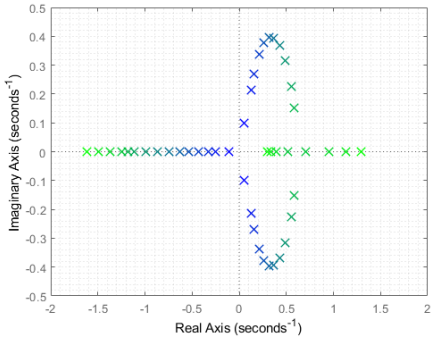

Figure 4: Poles for the vertical section (up to $t = 25\,\mathrm{s}$).

With the modal analysis some conclusions can be made. Firstly, the system is naturally unstable, which was expected due to negative static stability margin caused by the absence of aerodynamic fins. Secondly, during the vertical section, there is an equivalence between the lateral and longitudinal due to the symmetry of the vehicle and equality in nominal variables. Thirdly, the system displays natural oscillatory behaviour during the first seconds, after which all poles start to be located in the real axis. Finally, it is concluded that the velocity of the rocket is a driving factor for the dynamics of the system. At higher velocities the system is seen to have higher magnitude poles and hence faster dynamics.

4.2. Linear Quadratic Integral (LQI) Control

Using the linear time-varying state-space representation of the system, a linear quadratic regulator (LQR) is designed with the addition of an integral action, also known as linear quadratic integral control (LQI). The LQR is a technique that finds the optimal gain matrix $\mathbf{k}$ for the linear control law $\mathbf{u} = -\mathbf{k}\,\mathbf{x}$, which minimizes a quadratic cost function given by

$$J = \int_t^T [\,\mathbf{x}'(\tau)\,\mathbf{Q}\,\mathbf{x}(\tau) + \mathbf{u}'(\tau)\,\mathbf{R}\,\mathbf{u}(\tau)\,]\,d\tau\,, \quad (23)$$

where $\mathbf{Q}$ is a positive semi-definite matrix and $\mathbf{R}$ is a positive definite matrix. In the cost function, the quadratic form $\mathbf{x'Qx}$ represents a penalty on the deviation of the state x from the origin, and the term $\mathbf{u'Ru}$ represents the cost of control, making $\mathbf{Q}$ and $\mathbf{R}$ the tuning parameters for the resultant controller. By using the infinite-horizon version, which means taking T as infinity, the solution which minimizes the cost function and guarantees closed-loop asymptotic stability is the constant gain matrix

$$\mathbf{k} = \mathbf{R}^{-1}\,\mathbf{B}^T\,\mathbf{P}\,, \quad (24)$$

where $\mathbf{P}$ is the solution to the Algebraic Riccati Equation (ARE),

$$\mathbf{P}\,\mathbf{A} + \mathbf{A}^T\,\mathbf{P} - \mathbf{P}\,\mathbf{B}\,\mathbf{R}^{-1}\,\mathbf{B}^T\,\mathbf{P} + \mathbf{Q} = 0\,. \quad (25)$$

Since the system is time-varying, the ARE has to be solved for models coming from each linearization point, resulting in a set of gain matrices to be selected, or scheduled, throughout the flight.

The LQR feedback control law ideally drives the states of the system in the perturbation domain to zero, ensuring that the nominal values throughout the trajectory are followed. However, it does not guarantee a zero tracking error for non-zero references in terms of attitude. In order to have a zero reference tracking error, and to increase the robustness of the controller, an integral action that acts on the attitude tracking error is added, according to the scheme in Fig. 5.

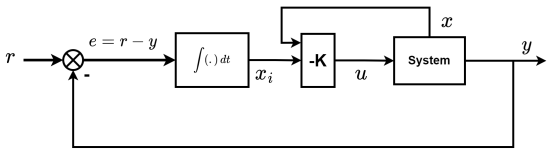

Figure 5: LQI control scheme.

Let the difference between the reference signal, r, and the output of the system, y, (the tracking error) be the time derivative of the state-space variable that results from adding the referred integrator, x_i. The state-space representation of the resulting regulator can be obtained by combining the open-loop state-space representation with the feedback law,

$$\dot{\mathbf{z}} = \left(\begin{bmatrix} \mathbf{A} & \mathbf{0} \\ -\mathbf{C} & \mathbf{0} \end{bmatrix} - \begin{bmatrix} \mathbf{B} \\ \mathbf{0} \end{bmatrix} \mathbf{K} \right) \mathbf{z} + \begin{bmatrix} \mathbf{0} \\ 1 \end{bmatrix} r\,, \quad (26)$$

where $\mathbf{z} = [\mathbf{x}\ x_i]^T$ is the augmented state vector and $\mathbf{C}$ is the output matrix that selects the output of the system from the original state vector ($y = \mathbf{C}\,\mathbf{x}$). The optimal gain $\mathbf{K}$ is obtained by solving the ARE using the rearranged system matrices,

$$\overline{\mathbf{A}} = \begin{bmatrix} \mathbf{A} & \mathbf{0} \\ -\mathbf{C} & \mathbf{0} \end{bmatrix}\,, \quad \overline{\mathbf{B}} = \begin{bmatrix} \mathbf{B} \\ \mathbf{0} \end{bmatrix}\,. \quad (27)$$

4.2.1. Implementation in the linear domain

Considering the decoupling between the longitudinal and lateral modes, the decoupled augment state vectors are

$$\delta\mathbf{z}_{lon} = [\delta u\ \ \delta w\ \ \delta q\ \ \delta\theta\ \ \delta\theta_i]^T, \quad (28a)$$

$$\delta\mathbf{z}_{lat} = [\delta v\ \ \delta r\ \ \delta\psi\ \ \delta\psi_i]^T, \quad (28b)$$

where $\delta\theta_i$ and $\delta\psi_i$ are the integral states. This implies that the $\mathbf{A}$, $\mathbf{B}$ are divided into the longitudinal and lateral modes, and that the $\mathbf{C}$ matrix for the lateral mode is the one that selects the yaw angle, while for the longitudinal mode is the one that selects the pitch angle.

The design degree of freedom is the selection of the tuning matrices $\mathbf{Q}$ and $\mathbf{R}$, which will also be divided into the longitudinal and lateral mode. First of all, setting all non-diagonal entries to zero, and only focusing on the diagonal ones, allows for a more intuitive matrix selection given by the "penalty" method. According to this method, the diagonal entries of the $\mathbf{Q}$ matrix will determine the relative importance of the state variables in terms of origin tracking performance, while the diagonal entries of the $\mathbf{R}$ matrix allow to directly adjust the control effort for each input. Therefore, the weighting matrices have the following generic format, separated for each mode

$$\mathbf{Q_{lon}} = diag\,(q_u,\ q_w,\ q_q,\ q_\theta,\ q_{\theta_i})\,, \quad (29a)$$

$$\mathbf{Q_{lat}} = diag\,(q_v,\, q_r,\, q_\psi,\, q_{\psi_i})\,, \tag{29b}$$

$$R_{lon} = r_{\mu_1}, \quad R_{lat} = r_{\mu_2}\,, \tag{29c}$$

Given the nature of the TVC actuation, trying to control the linear velocities will conflict with the attitude control, specially for non-zero attitude references. Hence, the linear velocity related terms are set as zero. By doing this, the associated gains will have negligible magnitude, allowing to use partial state feedback with,

$$\mathbf{k_{lon}} = [k_q \;\; k_\theta \;\; k_{\theta_i}]\,, \quad \mathbf{k_{lat}} = [k_r \;\; k_\psi \;\; k_{\psi_i}]\,. \tag{30}$$

The tuning parameters are iteratively adjusted looking at the closed-loop poles and at the step response performance in the linear domain, including the actuator dynamics, modelled as a first-order system. Regarding the closed-loop poles, the control law allowed to stabilize all operating points, placing all closed-loop poles in the left-hand side of the complex plane. Table 3 details the step response parameters for multiple operating points.

Table 3: Closed-loop step response parameters.

Op. point	Rise time (s)	Settling time (s)	Overshoot (%)
$t = 5\,$s	0.2686	0.4461	0.5710
$t = 35\,$s	0.3401	0.5723	0.1239
$t = 65\,$s	0.3278	0.5303	1.7586
$t = 95\,$s	0.3667	0.6052	0.7995

4.3. Linear Parameter Estimator

The robustness of the LQR is limited since the controller is designed considering a nominal evolution of model parameters that might considerably differ from the real evolution during the mission. Amongst the model parameters, the ones related with the aerodynamic properties of the rocket are subjected to an higher level of uncertainty, due to the difficulty in obtaining accurate aerodynamic coefficients and derivatives of the rocket for a broad range of velocities and aerodynamic angles. In this way, an online parameter estimator is proposed so that the controller acts on an informed value of the aerodynamic parameters. The aerodynamic parameters are hidden under the aerodynamic force and moment coefficients. Since a first estimate on these quantities is available using the stored aerodynamic data, a proportional error factor is multiplied in each aerodynamic force and moment and then estimated.

4.3.1. Estimator design

The estimator design follows along the methodology proposed in [10], where an hovercraft control system is designed based on dynamics parameter identification, which details a generic parameter estimator for time-varying systems, linear in the parameters.

The proportional error factors, δ_{a_x}, δ_{a_y}, δ_{a_z}, δ_m, and δ_n are included on the aerodynamic forces and moments,

$${}^B\mathbf{F_a} = \begin{bmatrix} -\overline{q}\,C_A\,S\delta_{a_x} \\ \overline{q}\,C_Y\,S\delta_{a_y} \\ -\overline{q}\,C_N\,S\delta_{a_z} \end{bmatrix} \; {}^B\mathbf{M_a} = \begin{bmatrix} 0 \\ \overline{q}\,C_m S\,d\delta_m \\ \overline{q}\,C_n S\,d\delta_n \end{bmatrix} \tag{31}$$

where the aerodynamic rolling moment is discarded due to the additional roll control system. After substituting the rearranged aerodynamic forces and moments in the rocket model, and considering the linearity in the parameters to be estimated, the nonlinear differential equations take the form,

$$\dot{\mathbf{x}} = \mathbf{f}(\mathbf{x}, t) + \mathbf{G}(\mathbf{x}, t)\,\boldsymbol{\zeta}\,, \tag{32}$$

where $\mathbf{x} = [u \;\; v \;\; w \;\; q \;\; r \;\; \phi \;\; \theta \;\; \psi]^T$ and $\boldsymbol{\zeta} = \left[\delta_{a_x} \;\; \delta_{a_y} \;\; \delta_{a_z} \;\; \delta_m \;\; \delta_n\right]^T$. Using state augmentation with the parameter vector, $\boldsymbol{\zeta}$, and assuming full state measurements, $\mathbf{y}$, are available, this system can be written in state-space form as

$$\begin{bmatrix} \dot{\mathbf{x}} \\ \dot{\boldsymbol{\zeta}} \end{bmatrix} = \begin{bmatrix} 0 & \mathbf{G}(\mathbf{y}, t) \\ 0 & 0 \end{bmatrix} \begin{bmatrix} \mathbf{x} \\ \boldsymbol{\zeta} \end{bmatrix} + \begin{bmatrix} \mathbf{f}(\mathbf{y}, t) \\ 0 \end{bmatrix}. \tag{33}$$

in which the full state measurement assumption allows to regard the system as linear, and the parameters are assumed to be slowly varying. The $\mathbf{G}(\mathbf{y}, t)$ and $\mathbf{f}(\mathbf{y}, t)$ matrices are easily obtained using the derived rocket model with the inclusion of the correction factors and so are not here presented to improve readability.

In order to design the estimator for this system, it is necessary for it to be observable. In the reference, it is demonstrated that the system is observable if and only if there exists no unit vector d, with the dimension of the parameter vector, such that

$$\int_{t_0}^{t} \mathbf{G}(\mathbf{y}, \sigma)\,d\sigma \cdot \mathbf{d} = 0. \tag{34}$$

Taking the time derivative in both sides and substituting for the rocket dynamics, the equivalent non-observability condition is

$$\begin{cases} -m^{-1}\,\overline{q}\,S\,C_A\,d_1 = 0 \\ m^{-1}\,\overline{q}\,S\,C_Y\,d_2 = 0 \\ -m^{-1}\,\overline{q}\,S\,C_N\,d_3 = 0 \\ J^{-1}\,\overline{q}\,S\,d\,C_m\,d_4 = 0 \\ J^{-1}\,\overline{q}\,S\,d\,C_n\,d_5 = 0 \end{cases} \Leftrightarrow \begin{cases} C_A\,d_1 = 0 \\ C_Y\,d_2 = 0 \\ C_N\,d_3 = 0 \\ C_m\,d_4 = 0 \\ C_n\,d_5 = 0 \end{cases} \tag{35}$$

where d_i, for $i = 1, 2, 3, 4, 5$, are the components of the unit vector, and the simplification is due to m, J, $\overline{q}$, d, and S being always different from zero.

It is possible to infer that the system is observable only when the aerodynamic force and moment coefficients are all different from zero, since if one of them is not, the unit vector with $d_i = 1$, where i

corresponds to component multiplying the null coefficient, satisfies the non-observability condition. However, given a null coefficient, the correspondent correction factor is the unobservable parameter, meaning that estimates can still be obtained for the remaining ones. Nevertheless, to ensure full observability, if the pre-calculation of a given coefficient results in zero, it can be forced to a small non-zero value. After verifying that the system can be made observable, a Kalman filter represents simple and easily tunable solution for the estimation of the system state.

4.3.2. Adaptive LQI control

By using the designed linear parameter estimator, the LQI controller gains can be computed on-board recurring to the real-time estimates of the aerodynamic correction factors. Instead of referring to the nominal evolution of the aerodynamic parameters and pre-calculate the gains to be scheduled during the flight, the gains are computed online. This is done by rewriting the state-space representation, including the estimated parameters, and solving the ARE onboard, with the updated state-space models. The rewriting of the system dynamics matrix, $\mathbf{A}$, can be easily achieved and is not here presented.

5. Navigation System Design

So far, it was assumed that the developed control system had access to an exact full-state measurement. In reality, it is necessary to have a navigation system, composed by sensors and estimators, capable of providing an accurate estimate on the state vector. For the case of rockets, and taking into account the state variables to measured, it is common to use an Inertial Measurement Unit (IMU), composed by accelerometers, gyroscopes, barometers, and magnetometers, and a Global Navigation Satellite System (GNSS) receiver.

5.1. Estimator Architecture

The estimator architecture was based on [11]. It is composed by three main filters, according to the scheme in Fig. 6. The first is an Attitude Complementary Filter (ACF), which in this case will use the Euler angles readings ($\boldsymbol{\lambda}_r$), obtained through the combination of a magnetometer and accelerometer, and the measured angular rates from the gyroscopes ($\boldsymbol{\omega}_r$) to provide a filtered attitude estimate ($\hat{\boldsymbol{\lambda}}$) and an estimate of the angular rate bias ($\mathbf{b}_\omega$) to correct the signal from the sensor. Dynamic acceleration will cause errors in the pitch and yaw measurements by the accelerometer. In this way, a pre-processing is done using the GNSS measured velocity to account for the dynamic acceleration. The second one is a Position Complementary Filter (PCF), which merges the position reading from the GNSS receiver, translated into the inertial frame ($\mathbf{P}_r$), and the accelerations measurements from the accelerometer ($\mathbf{a}_r$) to provide an estimate of the velocity components. This filter is also self-calibrated since it accounts for the bias in the accelerometer ($\mathbf{b}_a$). Finally, the last filter is the previously detailed linear parameter estimator (LPE), which will use the velocity, angular rate and attitude prefiltered values to give a final estimate on the state vector ($\hat{\mathbf{x}}$) and parameters ($\hat{\boldsymbol{\zeta}}$).

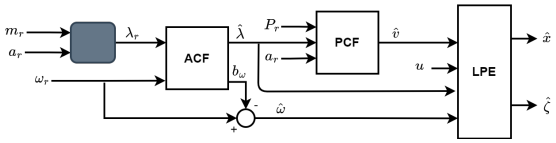

Figure 6: Estimator Architecture.

5.1.1. ACF

For the ACF, it is assumed that the Euler angles measurement is corrupted by Gaussian white-noise as well as the angular rates reading, and that the gyroscope bias is described by a constant term with additional Gaussian white-noise. Considering this, the filter is based on the kinematic equations for the Euler angles (19), using directly the Euler angles readings in the process matrices to allow for the use of a linear estimator, in this case a Kalman filter. Its state-space representation follows,

$$\dot{\hat{\mathbf{x}}} = \begin{bmatrix} 0 & 0 & 0 & -1 & -s_{\phi_r}\, t_{\theta_r} & 0 \\ 0 & 0 & 0 & 0 & -c_{\phi_r} & s_{\phi_r} \\ 0 & 0 & 0 & 0 & -\dfrac{s_{\phi_r}}{c_{\theta_r}} & -\dfrac{c_{\phi_r}}{c_{\theta_r}} \\ 0 & 0 & 0 & 0 & 0 & 0 \\ 0 & 0 & 0 & 0 & 0 & 0 \\ 0 & 0 & 0 & 0 & 0 & 0 \end{bmatrix} \hat{\mathbf{x}} + \\ + \begin{bmatrix} 1 & s_{\phi_r}\, t_{\theta_r} & 0 \\ 0 & c_{\phi_r} & -s_{\phi_r} \\ 0 & \dfrac{s_{\phi_r}}{c_{\theta_r}} & \dfrac{c_{\phi_r}}{c_{\theta_r}} \\ 0 & 0 & 0 \\ 0 & 0 & 0 \\ 0 & 0 & 0 \end{bmatrix} \boldsymbol{\omega}_r + \mathbf{K}\left(\mathbf{y} - \hat{\mathbf{y}}\right), \tag{36a}$$

$$\mathbf{x} = \begin{bmatrix} \boldsymbol{\lambda} & \mathbf{b}_\omega \end{bmatrix}^T, \quad \mathbf{y} = \lambda_\mathbf{r} + \mathbf{w}_\lambda, \quad \hat{\mathbf{y}} = \hat{\lambda}. \tag{36b}$$

To calculate the gain matrix $\mathbf{K}$, the time-invariant equivalent of the system is obtained by choosing the vertical attitude, $\boldsymbol{\lambda} = [0\ 0\ 0]^T$, to define the process matrices and compute the time-invariant Kalman gains.

5.1.2. PCF

For the PCF, both the position and acceleration measurements are considered to be corrupted by Gaussian white noise, and the accelerometer bias is also described by a constant term with additional Gaussian white noise. This filter is also kinematic,

considering the following equations of motion,

$$\dot{\mathbf{P}} = {}^{E}\mathbf{v}\,, \quad {}^{E}\dot{\mathbf{v}} = \mathbf{R}\ {}^{B}\mathbf{a}\,. \tag{37}$$

The state-space representation of the filter is then obtained,

$$\dot{\hat{\mathbf{x}}} = \begin{bmatrix} \mathbf{0} & \mathbf{I} & \mathbf{0} \\ \mathbf{0} & \mathbf{0} & -\mathbf{R} \\ \mathbf{0} & \mathbf{0} & \mathbf{0} \end{bmatrix} \hat{\mathbf{x}} + \begin{bmatrix} \mathbf{0} \\ \mathbf{R} \\ \mathbf{0} \end{bmatrix} \mathbf{a_r} + \begin{bmatrix} \mathbf{K_1} \\ \mathbf{K_2} \\ \mathbf{R}^T\,\mathbf{K_3} \end{bmatrix} (\mathbf{y} - \hat{\mathbf{y}})\,, \tag{38a}$$

$$\mathbf{x} = \begin{bmatrix} \mathbf{P} & {}^{E}\mathbf{v} & \mathbf{b_a} \end{bmatrix}^T\,, \quad \mathbf{y} = \mathbf{P_r} + \mathbf{w_P}\,, \quad \hat{\mathbf{y}} = \hat{\mathbf{P}}\,. \tag{38b}$$

The rotation matrix R is calculated using the Euler angles estimate from the ACF ($\hat{\boldsymbol{\lambda}}$). The individual gain matrices K_1, K_2 and K_3 can once again be computed considering the vertical attitude time-invariant to define the rotation matrix R, so as to obtain time-invariant kalman gains.

6. Simulation Results

6.1. Simulation Model

To test the proposed ADCS in the complete non-linear model, a simulation model is implemented in MATLAB/Simulink environment. The model is composed by several subsystems in order to completely transcribe the derived dynamics and kinematics.

6.2. LQI control

The LQI controller is implemented in the simulation model and tested by adding wind, with and without gusts, as external perturbation. Table 4 displays the results in terms of attitude tracking performance and control effort, not only for the LQI controller, but also for a tested PID controller for comparison.

Table 4: Tracking error and control effort.

	Average wind		Average wind + gusts	
	LQI	PID	LQI	PID
$\Sigma {\theta_e}^2$	3.15E-04	0.0173	2.6083	15.0879
$\Sigma {\psi_e}^2$	0.0016	1631.3	0.2457	1632.7
$\delta_{\mu_1,rms}$	0.2336	0.2299	0.6109	0.6125
$\delta_{\mu_2,rms}$	0.1512	177.88	0.3273	177.91

It is noted that the LQI controller provides better attitude tracking for the same control effort with respect to the PID. In the yaw plane, the results for the PID are significantly worse since it is very affected by the initial wind perturbation. The step response is also analysed (Tab. 5).

Table 5: Step response performance.

	$t = 5\,\mathrm{s}$				$t = 40\,\mathrm{s}$			
	LQI		PID		LQI		PID	
	θ	ψ	θ	ψ	θ	ψ	θ	ψ
Rise time (s)	0.26	0.26	0.77	0.50	0.32	0.25	0.70	0.58
Settling time (s)	0.48	0.48	3.54	2.85	0.56	0.46	5.92	4.65
Overshoot (%)	0.21	0.14	8.69	28.17	1.23	0.69	10.29	18.98

Once again the LQI displays satisfactory performance, close to the design values (3), and significantly better than the classical PID. Additionally, a robustness analysis is carried out, in which the model parameters are varied in percentage. For the assumed parameter uncertainties, the LQI controller shows high robustness.

6.3. LPE

The linear parameter estimator is also tested in simulation, by inducing errors in the aerodynamic coefficients, and is able to correctly estimate the parameters. Figure 7 presents the results for a simulation in which the aerodynamic corrections factors converge to the correct values.

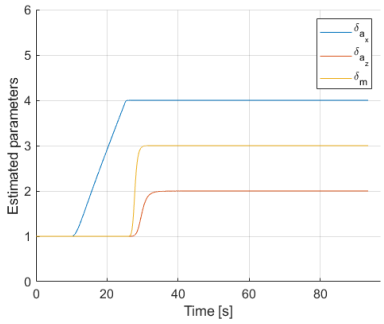

Figure 7: LPE simulation results.

6.3.1. Adaptive LQI control

Due to the high robustness of the regular LQI controller, the adaptive version is not able to produce significant performance improvements.

6.4. Navigation System

The navigation system is tested and is able to reject the noise introduced by the sensors, remove the bias, and provide an accurate estimate on the state of the rocket. Figure 8 presents the pitch angle estimation by the ACF, while Fig. 9 presents the position and velocity estimation by the PCF, both as exemplification of the performance of the system.

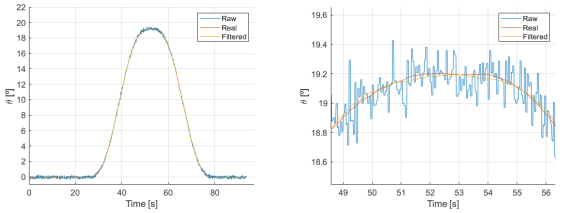

(a) Full trajectory

(b) Zoomed in the maximum pitch interval

Figure 8: ACF attitude estimation.

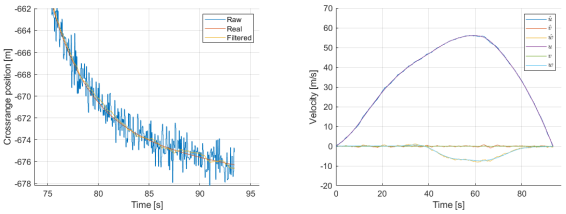

(a) Position estimation (b) Velocity estimation

Figure 9: PCF position and velocity estimation.

6.5. Complete ADCS

Finally, the complete ADCS system is tested by integrating the attitude control and navigation systems. Table 6 details the attitude tracking performance and the control effort with wind gusts present, in comparison with the results for the control system alone without sensor noise.

Table 6: ADCS simulation results.

	Control system alone	Complete ADCS
$\Sigma {\theta_e}^2$	2.6083	15.3665
$\Sigma {\psi_e}^2$	0.2457	11.9733
$\delta_{\mu_1,rms}$	0.6109	0.6309
$\delta_{\mu_2,rms}$	0.3273	0.3176

As expected, there is a performance decrease. However, it is still satisfactory.

7. Conclusions

With the conclusion of this work, it is possible to state that the primary goal has been achieved: the successful design of an attitude determination and control system applicable to sounding rockets with thrust vectoring. The design process was described in a generic way to ensure that the system can be easily applied to different vehicles under the same category. Nevertheless, the future implementation of the system in a student-built sounding rocket was always taken into account, as it was the initial motivation behind this work.

As future work, it would be of interest to develop non-linear controllers for the attitude control problem in order to compare the performance of said controllers with the developed ones. Particularly, the designed linear parameter estimator could be used for a non-linear control system that requires accurate information on the aerodynamic forces and moments to guarantee its correct functioning. Moreover, both the developed simulation model and navigation system can be verified and validated using real flight data from sounding rockets launched by RED. Finally, RED is currently developing small scale prototypes to test the TVC technology and the associated navigation and control systems. In this way, it is intended to implement the techniques in here developed to such prototypes and to analyse all the results coming from test campaigns.

References

[1] J W Cornelisse, H F R Schöyer, and K F Wakker. *Rocket Propulsion and Spaceflight Dynamics*. Pitman, 1979. ISBN:0-273-01141-3.

[2] V I Feodosiev and G B Siniarev. *Introduction to Rocket Technology*. Academic Press, 1959.

[3] Jiann Woei Jang, Abran Alaniz, Robert Hall, Nazareth Bedrossian, Charles Hall, and Mark Jackson. Design of launch vehicle flight control systems using ascent vehicle stability analysis tool. August 2011.

[4] George P. Sutton and Oscar Biblarz. *Rocket Propulsion Elements*. John Willey & Sons, 9^{th} edition, 2017. ISBN:9781118753880.

[5] Timothy Barrows and Jeb Orr. *Dynamics and Simulation of Flexible Rockets*. Academic Press, 2021. ISBN: 978-0-12-819994-7.

[6] Laura Sopegno, Patrizia Livreri, Margareta Stefanovic, and Kimon P. Valavanis. Linear quadratic regulator: A simple thrust vector control system for rockets. In *2022 30th Mediterranean Conference on Control and Automation (MED)*, pages 591–597, 2022.

[7] Ashish Tewari. *Advanced Control of Aircraft, Spacecraft and Rockets*. John Willey & sons, 2011. ISBN: 978-1-119-97120-7.

[8] YU Lei, ZHANG Yong-li, LI Teng-hui, and SUN Bin. A novel robust time-varying modal parameter estimation method based on absolute deviation for missile and rocket. In *2020 3rd World Conference on Mechanical Engineering and Intelligent Manufacturing (WCMEIM)*, pages 458–462, 2020.

[9] Wei Du, Bong Wie, and Mark Whorton. Dynamic modeling and flight control simulation of a large flexible launch vehicle. In *AIAA Guidance, Navigation and Control Conference & Exhibit*, August 2008.

[10] David Cabecinhas, Pedro Batista, Paulo Oliveira, and Carlos Silvestre. Hovercraft control with dynamic parameters identification. *IEEE Transactions on Control Systems Technology*, 26(3):785–796, 2018.

[11] André Antunes, Pedro Outeiro, Carlos Cardeira, and Paulo Oliveira. Implementation and testing of a sideslip estimation for a formula student prototype. *Robotics and Autonomous Systems*, 115:83–89, 2019.